Nuclear Science and Techniques (2026) 37:68
https://doi.org/10.1007/s41365-026-01903-8

Thermodynamics of heavy quarkonium in a Bayesian holographic QCD model

Li-Qiang Zhu[1] · Ou-Yang Luo[2] · Xun Chen[1,2,3,4] · Kai Zhou[5,6] · Han-Zhong Zhang[1] · De-Fu Hou[1]

Received: 13 September 2025 / Revised: 23 October 2025 / Accepted: 4 November 2025 / Published online: 31 January 2026

Abstract

Leveraging high-precision lattice QCD data on the equation of state and baryon number susceptibility at a vanishing chemical potential, we constructed a Bayesian holographic QCD model and systematically analyzed the thermodynamic properties of heavy quarkonium in QCD matter under varying temperatures and chemical potentials. We computed the quark-antiquark interquark distance, potential energy, entropy, binding energy, and internal energy. We present detailed posterior distribution results of the thermodynamic quantities of heavy quarkonium, including maximum a posteriori (MAP) value estimates and 95% confidence levels (CL). Through numerical simulations and theoretical analysis, we find that an increase in the temperature and chemical potential reduces the quark distance, thereby facilitating the dissociation of heavy quarkonium and leading to a suppressed potential energy. The increase in temperature and chemical potential also raises the entropy and entropy force, further accelerating the dissociation of heavy quarkonium. The calculated results of binding energy indicate that a higher temperature and chemical potential enhance the tendency of heavy quarkonium to dissociate into free quarks. The internal energy also increases with rising temperature and chemical potential. These findings provide significant theoretical insights into the properties of strongly interacting matter under extreme conditions and lay a solid foundation for the interpretation and validation of future experimental data. Finally, we also present the results for the free energy, entropy, and internal energy of a single quark.

Keywords Holographic QCD · Bayesian inference · In-medium heavy quarkonium · Thermodynamics of heavy quarkonium

1 Introduction

Ultra-relativistic heavy-ion collisions at the Relativistic Heavy Ion Collider (RHIC) and the Large Hadron Collider (LHC) are believed to have created a new state of matter known as the Quark–Gluon Plasma (QGP) [1–14]. In these extreme environments, heavy quark systems serve as sensitive probes, enabling the investigation of QGP properties and the underlying strong interaction dynamics governed by Quantum Chromodynamics (QCD) [15–21]. Heavy quark-antiquark pairs form bound states through strong interactions mediated by gluons. It has been pointed out that owing to the formation of the hot and dense QGP medium [22], these pairs have a maximum dissociation distance, beyond which the pair becomes unstable and separates. The interquark potential governs the formation and stability of these bound states. As the temperature and density intensify, the medium's color screening effect weakens the binding

This work was supported in part by the National Key Research and Development Program of China (No. 2022YFA1604900), the National Natural Science Foundation of China (NSFC) (Nos. 12405154, 12235016, 12221005, 12435009, 12275104, and 92570117), the Strategic Priority Research Program of Chinese Academy of Sciences (No. XDB34030000), the Fundamental Research Funds for the Central Universities, Open fund for Key Laboratories of the Ministry of Education (No.QLPL2024P01), CUHK-Shenzhen University Development Fund (Nos. UDF01003041 and UDF03003041), Shenzhen Peacock Fund (No. 2023TC0007), Ministry of Science and Technology of China (No. 2024YFA1611004), and the European Union–Next Generation EU through the research (No. P2022Z4P4B). "SOPHYA - Sustainable Optimized PHYsics Algorithms: fundamental physics to build an advanced society" under the program PRIN 2022 PNRR of the Italian Ministero dell'Università e Ricerca (MUR).

Extended author information available on the last page of the article

potential between heavy quarks, prompting dissociation—a hallmark phenomenon signifying the transition from confinement to deconfinement. Hence, exploring the in-medium heavy quark potential has emerged as a pivotal endeavor for deepening our understanding of hadronic structure and shedding light on the fundamental nature of QCD matter. Furthermore, the concept of the holographic potential for heavy quark-antiquark pairs was systematically introduced for the first time in [23], providing a theoretical foundation for investigating the structure of hadrons and the dynamics of QCD [17, 18, 24–47].

Heavy-ion collisions thus provide a unique and powerful experimental setting for probing QCD matter under extreme conditions. However, fully interpreting these experiments through lattice QCD simulations at finite chemical potentials is hindered by the fermion sign problem [48, 49], which severely limits numerical calculations in regions of high density. Although several innovative methodologies [50–61] have been developed to circumvent this obstacle, a complete and rigorous first-principles theoretical description of strongly coupled QCD matter under experimental conditions remains elusive. Consequently, complementary theoretical frameworks, particularly holographic QCD approaches inspired by the gauge/gravity duality from string theory, have gained prominence. Presently, the "top-down" approach is centered on constructing a realistic holographic QCD theory derived from string theory [62–66], whereas the "bottom-up" approach prioritizes the development of holographic model [67–73] informed by experimental observations and lattice QCD data. For instance, the incorporation of black hole configurations in five-dimensional spacetime to elucidate boundary phenomena at finite temperatures, along with the exploration of broader theoretical frameworks, constitutes pivotal research directions in this field [34, 38, 74–79].

Within the framework of holographic theory, the dissociation of heavy quark bound states in QGP medium have been extensively studied [80, 81]. These heavy quark bound states can be geometrically represented by open strings [82, 83] whose endpoints correspond to a heavy quark and antiquark pair located at the spacetime boundary, separated by an inter-quark distance L. In such models, the thermodynamics of QCD matter at finite temperature is mapped onto a five-dimensional black hole geometry, where the gravitational attraction of the black hole horizon dynamically captures the medium-induced effects experienced by the heavy quark-antiquark string. The string serves as a geometric representation of a bound state in QCD within the holographic framework. Initially, the string remains static at the boundary. However, influenced by the gravitational effects of the background spacetime metric, the string is gradually drawn toward the black hole's event horizon. This dynamic evolution of the string captures the microscopic mechanisms underlying the quark pair dissociation. As the string approaches the horizon, the system achieves equilibrium, and the binding energy of the string diminishes to a critical value, resulting in the dissociation of the quark-antiquark pair. The timescale associated with this process, known as dissociation time of the quark-antiquark pair, is a critical parameter in the study of quarkonium suppression and provides a key indicator of the non-equilibrium properties of strongly interacting media under extreme conditions. This timescale provides essential theoretical insights into the formation and evolution of the QGP. Moreover, examining the variations in the dissociation time not only helps elucidate the strongly coupled dynamics of QCD but also explains the experimentally observed suppression of heavy quarkonium states. Such analyses significantly enhance our understanding of matter under extreme conditions in high-energy nuclear physics.

Based on the holographic QCD models described in prior works [84–86], the main research objective of this study is to analyze the impact of varying temperature and chemical potential on the thermodynamic properties of heavy quarkonium in a 2+1 flavor system. The remainder of this paper is organized as follows: Sect. 2 provides a brief review of the holographic model that incorporates information about the QCD phase transition. In Sect. 3, we analyze the dissociation distance, potential energy, entropy, entropy force, binding energy, and internal energy of the heavy quark-antiquark pair under different temperature and chemical potential conditions. Section 4 examines the effects of temperature and chemical potential on the thermodynamic properties of a single quark. Finally, Sect. 5 summarizes the research findings and presents the concluding remarks.

2 The setup

This section provides an overview of the Einstein–Maxwell–dilaton (EMD) model. Within the context of the string frame, the action for the EMD model reads [17, 18, 42, 44, 46, 84, 85, 87–90]

$$S_b = \frac{1}{16\pi G_5}\int \mathrm{d}^5x\sqrt{-g^{\mathrm{s}}}e^{-2\phi_{\mathrm{s}}} \times\left[R_{\mathrm{s}} - \frac{f_{\mathrm{s}}(\phi_{\mathrm{s}})}{4}F^2 + 4\partial_\mu\phi_{\mathrm{s}}\partial^\mu\phi_{\mathrm{s}} - V_{\mathrm{s}}(\phi_{\mathrm{s}})\right]. \tag{1}$$

Here, ϕ is a neutral dilaton scalar field. $f(\phi)$ is the gauge kinetic function coupled to the Maxwell field A_μ, and $V(\phi)$ defines the dilaton field's potential. Parameter G_5 corresponds to the Newton constant in five-dimensional spacetime. By solving the equations of motion (EoMs), the functional forms of $f(\phi)$ and $V(\phi)$ can be determined consistently. The action is rewritten in the Einstein frame from the string frame through a specific set of transformations.

$$\phi_{\rm s}=\sqrt{\frac{3}{8}}\phi,\quad g^{\rm s}_{\mu\nu}=g_{\mu\nu}e^{\sqrt{\frac{2}{3}}\phi},\quad f_{\rm s}(\phi_{\rm s})=f(\phi)e^{\sqrt{\frac{2}{3}}\phi},\\ V_{\rm s}(\phi_{\rm s})=e^{-\sqrt{\frac{2}{3}}\phi}V(\phi). \tag{2}$$

In the Einstein frame, the action is expressed as:

$$S_b=\frac{1}{16\pi G_5}\int {\rm d}^5x\sqrt{-g}\\ \times\left[R-\frac{f(\phi)}{4}F^2-\frac{1}{2}\partial_\mu\phi\partial^\mu\phi-V(\phi)\right]. \tag{3}$$

We propose the following metric ansatz:

$${\rm d}s^2=\frac{L^2e^{2A(z)}}{z^2}\left[-g(z){\rm d}t^2+\frac{dz^2}{g(z)}+{\rm d}\vec{x}^2\right]. \tag{4}$$

In this context, z serves as the holographic coordinate in the fifth dimension, and the AdS_5 space is characterized by a fixed radial parameter $R_{\rm AdS}=1$. By employing the aforementioned metric ansatz, one can derive the corresponding equations of motion and constraints for the background fields

$$\phi''+\phi'\left(-\frac{3}{z}+\frac{g'}{g}+3A'\right)-\frac{e^{2A}}{z^2g}\frac{\partial V}{\partial\phi}\\ +\frac{z^2e^{-2A}A_{\rm t}'^2}{2g}\frac{\partial f}{\partial\phi}=0, \tag{5}$$

$$A_{\rm t}''+A_{\rm t}'\left(-\frac{1}{z}+\frac{f'}{f}+A'\right)=0, \tag{6}$$

$$g''+g'\left(-\frac{3}{z}+3A'\right)-\frac{e^{-2A}A_{\rm t}'^2z^2f}{L^2}=0, \tag{7}$$

$$A''+\frac{g''}{6g}+A'\left(-\frac{6}{z}+\frac{3g'}{2g}\right)-\frac{1}{z}\left(-\frac{4}{z}+\frac{3g'}{2g}\right)\\ +3A'^2+\frac{e^{2A}V}{3z^2g}=0, \tag{8}$$

$$A''-A'\left(-\frac{2}{z}+A'\right)+\frac{\phi'^2}{6}=0. \tag{9}$$

Among these five equations, only four are independent in a linear sense. The infrared (IR) boundary conditions for the equations of motion (EoMs) near the horizon ($z=z_{\rm h}$) represent the boundary of the black hole, which is physically associated with the concept of temperature. This can be expressed as

$$A_{\rm t}(z_{\rm h})=g(z_{\rm h})=0. \tag{10}$$

As the IR boundary is approached $z\to z_{\rm h}$, we impose the condition that the metric in the string frame converges to AdS_5. The conditions at the ultraviolet (UV) boundary ($z=0$) are as follows:

$$A(0)=-\sqrt{\frac{1}{6}}\phi(0),\quad g(0)=1,\quad A_{\rm t}(0)=\mu+\rho' z^2+\cdots, \tag{11}$$

where μ denotes the baryon chemical potential, while ρ' scales proportionally with the baryon number density, The baryon number density can be calculated based on [91, 92]

$$\rho=\left|\lim_{z\to0}\frac{\partial\mathcal{L}}{\partial(\partial_z A_{\rm t})}\right|\\ =-\frac{1}{16\pi G_5}\lim_{z\to0}\left[\frac{{\rm e}^{A(z)}}{z}f(\phi)\frac{\rm d}{{\rm d}z}A_{\rm t}(z)\right]. \tag{12}$$

μ is related to the quark-number chemical potential $\mu=3\mu_{\rm q}$. This allows us to derive

$$g(z)=1-\frac{1}{\int_0^{z_{\rm h}}{\rm d}x x^3e^{-3A(x)}}\\ \times\left[\int_0^z{\rm d}x x^3e^{-3A(x)}+\frac{2c\mu^2e^k}{(1-e^{-cz_{\rm h}^2})^2}{\rm det}\mathcal{G}\right], \tag{13}$$

$$\phi'(z)=\sqrt{6\left(A'^2-A''-\frac{2}{z}A'\right)}, \tag{14}$$

$$A_{\rm t}(z)=\mu\frac{e^{-cz^2}-e^{-cz_{\rm h}^2}}{1-e^{-cz_{\rm h}^2}}, \tag{15}$$

$$V(z)=-3z^2ge^{-2A}\left[A''+A'\left(3A'-\frac{6}{z}+\frac{3g'}{2g}\right)\right.\\ \left.-\frac{1}{z}\left(-\frac{4}{z}+\frac{3g'}{2g}\right)+\frac{g''}{6g}\right], \tag{16}$$

where

$$\det\mathcal{G}=\begin{vmatrix}\int_0^{z_{\rm h}}{\rm d}y y^3e^{-3A(y)} & \int_0^{z_h}{\rm d}y y^3e^{-3A(y)-cy^2}\\ \int_{z_{\rm h}}^{z}{\rm d}y y^3e^{-3A(y)} & \int_{z_h}^{z}{\rm d}y y^3e^{-3A(y)-cy^2}\end{vmatrix}. \tag{17}$$

The Hawking temperature [93, 94] is defined by

$$T=\frac{|g'(z)|}{4\pi}\\ =\frac{z_{\rm h}^3e^{-3A(z_{\rm h})}}{4\pi\int_0^{z_{\rm h}}{\rm d}y y^3e^{-3A(y)}}\\ \left[1+\frac{2c\mu^2e^k\left(e^{-cz_{\rm h}^2}\int_0^{z_{\rm h}}{\rm d}y y^3e^{-3A(y)}-\int_0^{z_h}{\rm d}y y^3e^{-3A(y)}e^{-cy^2}\right)}{(1-e^{-cz_{\rm h}^2})^2}\right]. \tag{18}$$

In order to achieve an analytical solution, we make use of

$$A(z) = d\ln(az^2 + 1) + d\ln(bz^4 + 1). \tag{19}$$

The gauge kinetic function $f(z)$ is defined as

$$f(z) = e^{cz^2 - A(z) + k}. \tag{20}$$

In the string frame, the potential of a quark-antiquark pair is determined via $A_s(z) = A(z) + \sqrt{\frac{1}{6}}\phi(z)$. Standard techniques enable the computation of their separation distance and interaction potential [30, 32, 40, 74, 79]. The dynamics of the string world-sheet are described by the Nambu–Goto action in the form shown below

$$S_{\mathrm{NG}} = -\frac{1}{2\pi\alpha'}\int \mathrm{d}^2\xi\sqrt{-\det g_{ab}}. \tag{21}$$

In this context, g_{ab} refers to the induced metric, defined as

$$g_{ab} = g^{\mathrm{s}}_{MN}\partial_a X^M \partial_b X^N, \quad a, b = 0, 1, \tag{22}$$

and α' is associated with the string tension and assigned a value of 1. In this context, X^M represents the coordinates, and g^{s}_{MN} denotes the metric in the string frame. To calculate the heavy quark-antiquark potential, the string is anchored at a static quark-antiquark pair located at $x_1 = -L/2$ and $x_1 = L/2$. The most straightforward parametrization of the string world-sheet coordinates is $\xi^0 = t$ and $\xi^1 = x_1$. In this scenario, the effective Nambu–Goto action can be represented as

$$S_{\mathrm{NG}} = -\frac{1}{2\pi T}\int_{-L/2}^{L/2}\mathrm{d}x_1\sqrt{k_1(z)\frac{\mathrm{d}z^2}{\mathrm{d}x_1^2} + k_2(z)}, \tag{23}$$

where

$$\begin{aligned} k_1 &= \frac{e^4 A_{\mathrm{s}}}{z^2}, \\ k_2 &= \frac{e^4 A_{\mathrm{s}}}{z^2} g(z). \end{aligned} \tag{24}$$

Based on the research in [28, 74, 95–98], the Wigner-Wilson loop's expectation value is linked to the on-shell string action by:

$$\langle W(\mathcal{C})\rangle = \int DX e^{-S_{\mathrm{NG}}} \simeq e^{-S_{\mathrm{on-shell}}}. \tag{25}$$

Here, $\mathcal{C}$ represents a closed loop in spacetime. The heavy quark potential is defined as [23, 39, 99]:

$$\langle W(\mathcal{C})\rangle =\sim e^{-V(r,T)/T}, \tag{26}$$

L denotes the distance between the quark-antiquark pair. Consequently, calculating the potential requires solving the on-shell string world-sheet action. Based on the standard framework [17, 28, 30, 32, 40, 46], we establish an effective "Hamiltonian".

$$\mathcal{H} = z'\frac{\partial\mathcal{L}}{\partial z'} - \mathcal{L} = \frac{k_2(z)}{\sqrt{k_1(z)z'^2 + k_2(z)}}. \tag{27}$$

Here, $z' = \frac{\mathrm{d}z}{\mathrm{d}x_1}$, and solving for z' forms the equation

$$\frac{k_2(z)}{\sqrt{k_1(z)z'^2 + k_2(z)}} = \frac{k_2(z_0)}{\sqrt{k_2(z_0)}}. \tag{28}$$

Here, z_0 marks the vertex where the quark-antiquark string connects, with values from $z_0 = 0$ to $z_0 = z_{\mathrm{h}}$. This allows us to calculate the interquark distance and the potential energy,

$$\begin{aligned} L &= \int_{-\frac{L}{2}}^{\frac{L}{2}}\mathrm{d}x = 2\int_0^{z_0}\mathrm{d}z\frac{1}{z'} \\ &= 2\int_0^{z_0}\left[\frac{k_2(z)}{k_1(z)}\left(\frac{k_2(z)}{k_2(z_0)} - 1\right)\right]^{-1/2}\mathrm{d}z, \end{aligned} \tag{29}$$

$$\begin{aligned} V_{Q\bar{Q}} = \frac{1}{\pi}\Bigg(&\int_0^{z_0}\mathrm{d}z\left(\sqrt{\frac{k_2(z) - k_1(z)}{k_2(z) - k_2(z_0)}} - \left(\frac{1}{z^2} + \frac{2\sqrt{-6ad}}{z}\right)\right) \\ &- \left(\frac{1}{z_0} - 2\sqrt{-6ad}\ln(z_0)\right)\Bigg). \end{aligned} \tag{30}$$

In our computational framework, the potential energy of the heavy quarkonium is equal to its free energy ($F_{Q\bar{Q}} = V_{Q\bar{Q}}$) [39, 100, 101]. The potential is regularized by subtracting the UV-divergent term.

The entropy of the quark-antiquark pair is derived as

$$S_{Q\bar{Q}} = -\frac{\partial F_{Q\bar{Q}}}{\partial T} = -\frac{\partial F_{Q\bar{Q}}}{\partial z_{\mathrm{h}}}\frac{\partial z_{\mathrm{h}}}{\partial T}, \tag{31}$$

where T represents the QGP temperature, and the binding energy can be given by [39]

$$E_{Q\bar{Q}} = F_{Q\bar{Q}} - 2F_Q, \tag{32}$$

F_Q represents the free energy of a single quark, which can be computed as shown in Ref. [18], with the integral's upper limit fixed at z_{h}. Specifically:

$$\begin{aligned} \frac{F_Q}{\sqrt{\lambda}} = \frac{1}{2\pi}\Bigg(&\int_0^{z_{\mathrm{h}}}\mathrm{d}z\left(\sqrt{k_1(z)} - \left(\frac{1}{z^2} + \frac{2\sqrt{-6ad}}{z}\right)\right) \\ &- \left(\frac{1}{z_{\mathrm{h}}} - 2\sqrt{-6ad}\ln(z_{\mathrm{h}})\right)\Bigg). \end{aligned} \tag{33}$$

In this study, we set $\sqrt{\lambda} = 1$ for convenience. The internal energy of the quark-antiquark pair, as described in Refs. [39, 102], is

$$U_{Q\bar{Q}} = F_{Q\bar{Q}} + TS_{Q\bar{Q}} + \mu N_{Q\bar{Q}}, \tag{34}$$

with $N_{Q\bar{Q}}$ related to the baryon number density.

For the 2+1 flavor system, the six parameters (a, b, c, d, k, G_5) in our model are derived from Ref. [86]. In Ref. [86], we obtained the posterior parameter distribution of the EMD model through Bayesian analysis, which integrates lattice QCD data $(S/T^3, \chi_2^B, C_s^2)$ at zero chemical potential [103, 104] within the EMD framework. The Bayesian analysis procedure consists of the following steps. First, based on Bayes' theorem:

$$P(\boldsymbol{\theta}|\text{data}) \propto P(\text{data}|\boldsymbol{\theta})P(\boldsymbol{\theta}), \tag{35}$$

$P(\boldsymbol{\theta}|\text{data})$ represents the posterior distribution, which is the conditional probability of the parameters given the observed data. $P(\boldsymbol{\theta})$ denotes the prior distribution, reflecting our initial assumptions or prior knowledge about the parameters. $P(\text{data}|\boldsymbol{\theta})$ refers to the likelihood function, that is, the probability of observing the data based on specific assumed parameter values. Here, "data" corresponds to the lattice QCD data $(S/T^3, \chi_2^B, C_s^2)$, while θ represents the parameters of the EMD model.

Then, for the prior distribution $P(\boldsymbol{\theta})$ pertaining to the EMD model parameters $\boldsymbol{\theta} = (a, b, c, d, k, G_5)$, we established a range of prior parameters based on Ref. [85], as detailed in Table 1 of Ref. [86]. Within this prior range, 300 parameter sets $\boldsymbol{\theta}$ were sampled using the Latin Hypercube Sampling (LHS) [105, 106]. These parameter sets were subsequently input into the EMD model to compute the observables S/T^3, χ_2^B, and C_s^2. The computation results were then processed via Principal Component Analysis (PCA) [107]. Finally, a Gaussian process emulator [108] was constructed by pairing the input 300 parameter sets with their corresponding PCA-transformed outputs for subsequent likelihood function development.

For the likelihood function $P(\text{data}|\boldsymbol{\theta})$, we employed a Gaussian distribution:

$$P(\text{data}|\boldsymbol{\theta}) = \prod_i \frac{1}{\sqrt{2\pi}\sigma_i} e^{-\frac{[y_i(\boldsymbol{\theta}) - y_i^{\text{lattice}}]^2}{2\sigma_i^2}}, \tag{36}$$

y_i^{lattice} represents the lattice QCD data, $y_i(\boldsymbol{\theta})$ denotes the output values of the EMD model, where the EMD model is replaced by a Gaussian processes emulator (to accelerate computational speed). σ_i represents the combined uncertainties from both the lattice QCD data and the Gaussian emulator. Finally, by performing Markov Chain Monte Carlo (MCMC) [109, 110] sampling on the posterior distribution, we obtained the posterior parameter distribution of the EMD model. As shown in Table 2, we present the 95% confidence level (CL) parameter ranges along with the maximum a posteriori (MAP) values [86].

Table 1 Parameter ranges for prior distribution in the EMD model [86]

Prior		
Parameter	Min	Max
a	0.110	0.310
b	0.005	0.031
c	−0.280	−0.205
d	−0.240	−0.110
k	−0.910	−0.770
G_5	0.375	0.430

3 Thermodynamics of heavy quarkonium

In this section, we systematically investigate the thermodynamic properties of heavy quark-antiquark pairs in a 2+1 flavor system, focusing on the effects of temperature and chemical potential on these properties to elucidate their behavior within a strongly interacting medium and the mechanism underlying their transition from the confined phase to the deconfined phase. Specifically, this chapter is divided into five subsections: (A) The interquark distance of heavy quark-antiquark pairs, in which we explore how the dissociation distance varies with temperature and chemical potential, as well as its relationship with confinement effects; (B) The potential energy of heavy quark-antiquark pairs, where we analyze the composition of the potential energy and the phenomenon of its truncation under the influence of temperature and chemical potential; (C) The entropy and entropy force of heavy quark-antiquark pairs, studying the variation of entropy with temperature and chemical potential to reveal the degree of disorder within the system; (D) The binding energy of heavy quark-antiquark pairs, investigating how the binding energy changes with temperature and chemical potential and its connection to quark dissociation; (E) The internal energy of heavy quark-antiquark pairs, analyzing the variation of internal energy with temperature and chemical potential and its role in thermodynamics. Through these studies, we aim to achieve a comprehensive understanding of the thermodynamic behavior of quark-antiquark pairs in a 2+1 flavor system.

3.1 The dissociation of heavy quark-antiquark pairs

In this subsection, we investigate the behavior of the interquark distance L of heavy quark-antiquark pairs in a 2+1 flavor system as a function of the z_0. Our calculated results of $L(z_0)$ with the maximum a posteriori (MAP) inference setup for the Bayesian holographic model [86] are depicted in Fig. 1, with Fig. 1 (a) shows the results of calculating the effect of different temperatures on L with the chemical potential fixed at zero, and Fig. 1 (b) shows the results of calculating the effect of the chemical potential on L with the temperature fixed at $T = 0.134$ GeV.

As illustrated in Fig. 1, it has been observed that the interquark distance L increases with z_0 until it reaches a peak value known as the dissociation distance $L_{\max}$. After this maximum point, further increases in z_0 lead to a decrease in the interquark distance, L. This trend suggests that the quark-antiquark pairs transition into a deconfined state, resulting in the melting of the string connecting them. Consequently, the bound state of the quark-antiquark pairs dissociates, and they eventually become free heavy quarks. This phenomenon highlights the color screening effect of the medium on these bound states, which means that partons in the medium (QGP) can "shield" the interactions between the quark and antiquark pairs, preventing their tight binding.

By analyzing the behavior of the dissociation distance, we found that as the temperature and chemical potential increased, the dissociation distance $L_{\max}$ gradually became smaller. This is related to the increasing parton density in the medium with increasing temperature and chemical potential, which thereby enhances the screening effect on the heavy quark bound states. This leads to a decrease in the dissociation distance, making it easier for the quark-antiquark pairs to enter a deconfined state and transition into free quarks.

Table 2 In the 2+1 flavor system, the 95% CL ranges and MAP values for the six model parameters a, b, c, d, k and G_5 are determined through Bayesian inference [86]

Posterior 95% CL			
Parameter	Min	Max	MAP
a	0.229	0.282	0.252
b	0.019	0.027	0.023
c	−0.261	−0.231	−0.245
d	−0.143	−0.127	−0.135
k	−0.871	−0.808	−0.843
G_5	0.388	0.406	0.397

3.2 Potential energy

In this subsection, we investigate the potential energy of heavy quark-antiquark pairs, a crucial physical quantity that characterizes the interaction between quark and antiquark. Recent pNRQCD [111] studies and one-loop hard-thermal-loop (HTL) calculations [112] have shown that the heavy quark potential at finite temperatures also develops a non-vanishing imaginary part, reflecting the Laudau damping and color singlet to octet transition. In holographic models, the imaginary part of the heavy quarkonium potential was first computed in Ref. [113]. In the holographic model employed in this study, similar methods to those in Ref. [113] could also be utilized to calculate the imaginary part of the potential. We plan to address the computation of the imaginary part in a future study, as this study serves as a preliminary exploratory analysis, where we first aim to examine the real part of the potential obtained through Bayesian analysis. Subsequently, we intend to further investigate the imaginary part of the potential in follow-up work, again using Bayesian analysis combined with the EMD model. Currently, in lattice QCD, there is no definitive consensus regarding either the temperature dependence of the heavy quarkonium potential or the precise forms of its real and imaginary parts, and this issue remains under active debate. For example, Ref. [114] applied four distinct methods to compute the real and imaginary parts of the potential, and the conclusions drawn from these four methods are not entirely consistent. Although we also plan to compute the imaginary part of the potential in

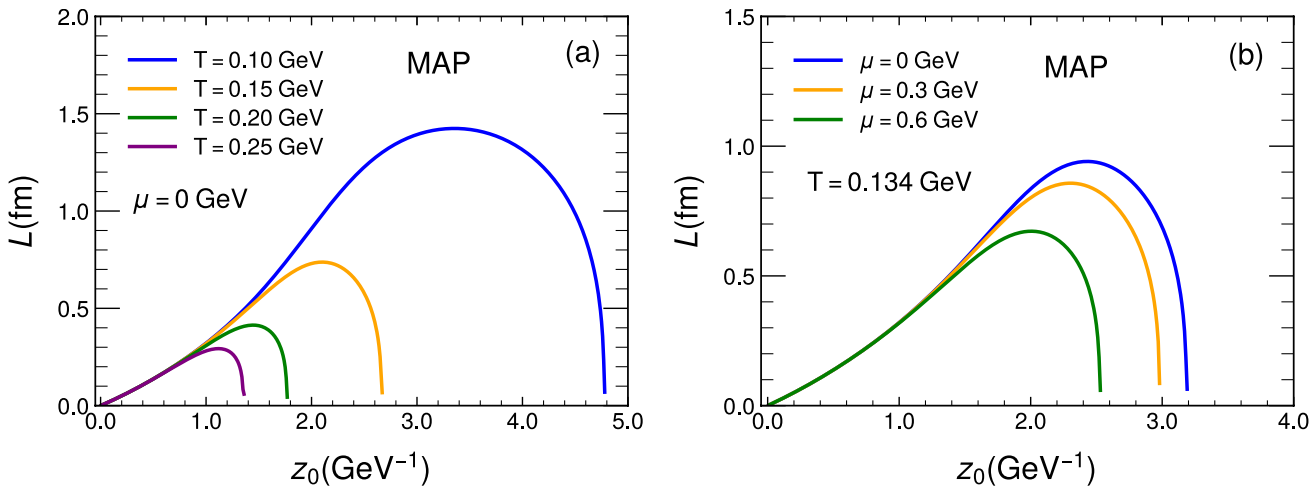

Fig. 1 (Color online) When selecting MAP setup for the Bayesian Holographic model, the calculated interquark distance L as a function of z_0 for the quark-antiquark pair at different temperatures when $\mu = 0$ (**a**) and at different chemical potential when $T = 0.134$ GeV (**b**)

our future work, how to directly compare it with lattice QCD results remains an open and debated question.

This real part of the potential energy typically consists of a short-range Coulomb potential and a long-range linear potential. At short distances, the Coulomb potential dominates, expressed as $F(r) \propto -\frac{\alpha}{r}$, where α is the effective coupling constant of the strong interaction. The Coulomb potential reflects the attractive force between the quark and antiquark, similar to the Coulomb potential in electromagnetic interactions, but is mediated by the color charge of the strong interaction. At long distances, the potential energy gradually shifts to being dominated by the linear potential, reflecting the binding mechanism of quark pairs, expressed as $F(r) \propto \sigma r$, where σ is the string tension constant. This linear potential represents the binding effect of the "string" formed by the gluon field between the quark and antiquark, corresponding to the manifestation of confinement and is a significant feature of the strong interaction, ensuring that quarks and antiquarks remain bound together at large distances.

As shown in Fig. 2, when the separation distance between quarks is very small, the potential energy is primarily influenced by the Coulomb potential, resulting in a negative value. As the quark separation distance increases, the potential energy gradually transitions to being dominated by the linear potential. In Fig. 2, we calculated the results for the 95% CL (shaded area) and the MAP (red solid line) setup, subfigure (a) displays the calculation results of the effect of different temperatures on the potential energy with the chemical potential fixed at zero, while subfigure (b) presents the calculation results of the effect of chemical potential on the potential energy with the temperature fixed at $T = 0.134$ GeV. Our calculations indicate that with an increase in the system temperature and chemical potential, the linear potential component of the quark pair slightly decreases but does not show a clear color screening effect. This phenomenon may be related to the tendency for quark pairs to dissociate owing to the increased thermal energy, which reduces the length of the linear component of the potential energy. Meanwhile, the Coulomb potential component remains almost unaffected, indicating that the short-range strong interactions remain stable under higher temperatures and chemical potentials. At extremely small interquark distances (typically far smaller than characteristic medium scales, such as the Debye screening length), the interaction enters the perturbative QCD regime. Under these conditions, the strong coupling constant becomes sufficiently small [115–117], rendering the potential energy predominantly governed by the Coulomb interaction mediated through single-gluon exchange. This perturbative mechanism is intrinsically dictated by the local quark-gluon dynamics of QCD. Consequently, across the temperature and chemical potential range considered in our study, medium modifications to the potential remained negligible. As shown in Fig. 3, we compare the results from our model with the recent lattice data [118], where the data points represent the lattice results, and the colored shaded regions along with the red lines depict our model's predictions, this comparison clearly depicts a significant resemblance between the Bayesian holographic model's results and the lattice data for heavy quark potential.

In our model, when computing the potential energy as a function of L at a specific temperature or chemical potential, there exists a dissociation distance $L_{\max}$. As shown in Fig. 1,

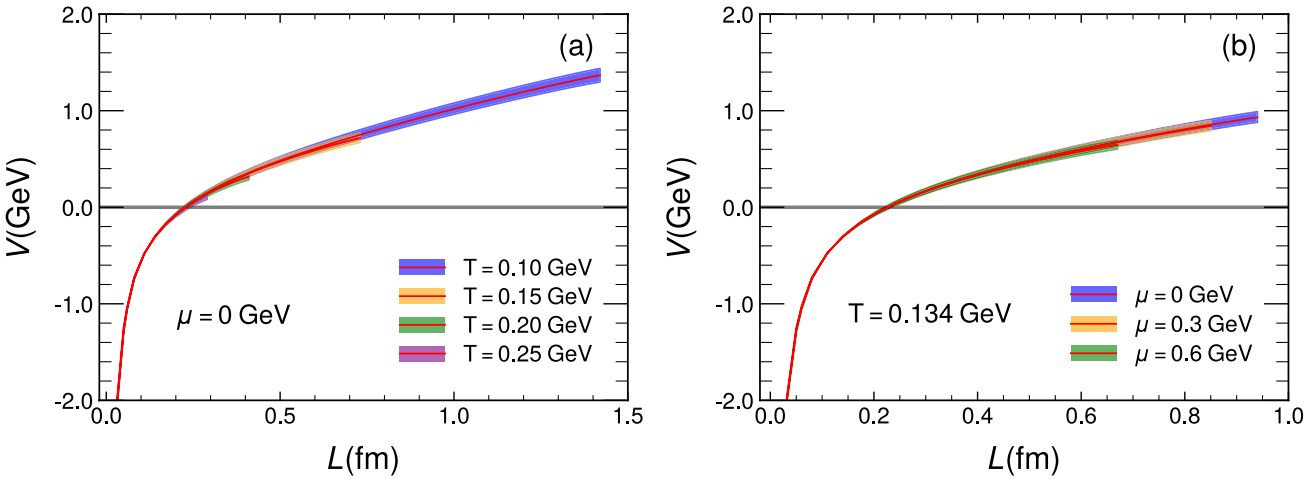

Fig. 2 (Color online) **a** The dependence of the potential energy V of quark-antiquark pairs on the interquark distance L at different temperatures when $\mu = 0$. **b** The dependence of the potential energy V of quark-antiquark pairs on the interquark distance L at different chemical potential when $T = 0.134$ GeV. The shaded area represents the 95% CL, and the red solid line denotes the result of the MAP calculation

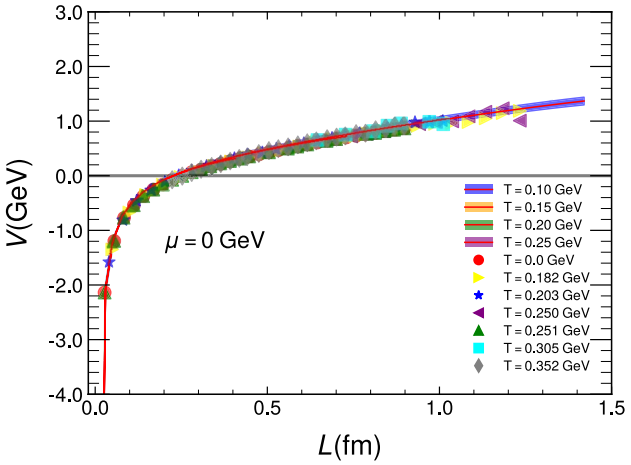

Fig. 3 (Color online) A comparison is made between the potential energy of quark-antiquark pairs from model calculation results and lattice data [118] for the case of $N_f = 2 + 1$ and $\mu = 0$. The lattice data are represented by various shapes of points. The shaded area represents the 95% CL, and the red solid line denotes the result of the MAP calculation

the peak value of the computed L corresponds to this dissociation distance. When L exceeds L_{max}, the bound state of the heavy quarkonium dissociates and ceases to exist. At a temperature of 0.25 GeV, the dissociation distance L_{max} is approximately 0.3 fm, which confines our calculated potential energy range to approximately $L \sim 0.3$ fm at this temperature. In Ref. [118], the real part of the lattice QCD potential does not exhibit screening behavior, indicating that it shows no signatures of dissociation. To account for the dissociation dynamics of heavy quarkonium in lattice QCD, it is necessary to incorporate both the real and imaginary parts of the potential. As an exploratory analysis, our comparison was confined to the real part of the lattice QCD results. Therefore, our model provides additional information in the form of the dissociation distance, which is not present in the lattice QCD data.

3.3 Entropy

In this subsection, we systematically investigate the entropy of heavy quark-antiquark pairs, an important physical quantity used to characterize the degree of disorder in the micro-states induced by the interactions between quarks and antiquarks. Entropy not only provides crucial insights into the thermodynamic properties of the heavy quark system but also reveals the underlying mechanisms of its dynamic behavior. The specific expression for the entropy is given by Eq. (31). Furthermore, we examine how the entropy varies with the interquark distance L and analyze its behavior under different temperature and chemical potential conditions. The relevant results are presented in Fig. 4, We calculated the results for the 95% CL (shaded area) and the MAP (red solid line), subfigure (a) displays the calculation results of the effect of different temperatures on the entropy with the chemical potential fixed at zero, while subfigure (b) presents the calculation results of the effect of chemical potential on the entropy with the temperature fixed at $T = 0.134$ GeV. Our research indicates that as the temperature and chemical potential increase, the value of the entropy also rises. This finding leads us to conclude that, in environments with higher temperature and chemical potential, the production rate of heavy quark-antiquark pairs is significantly suppressed.

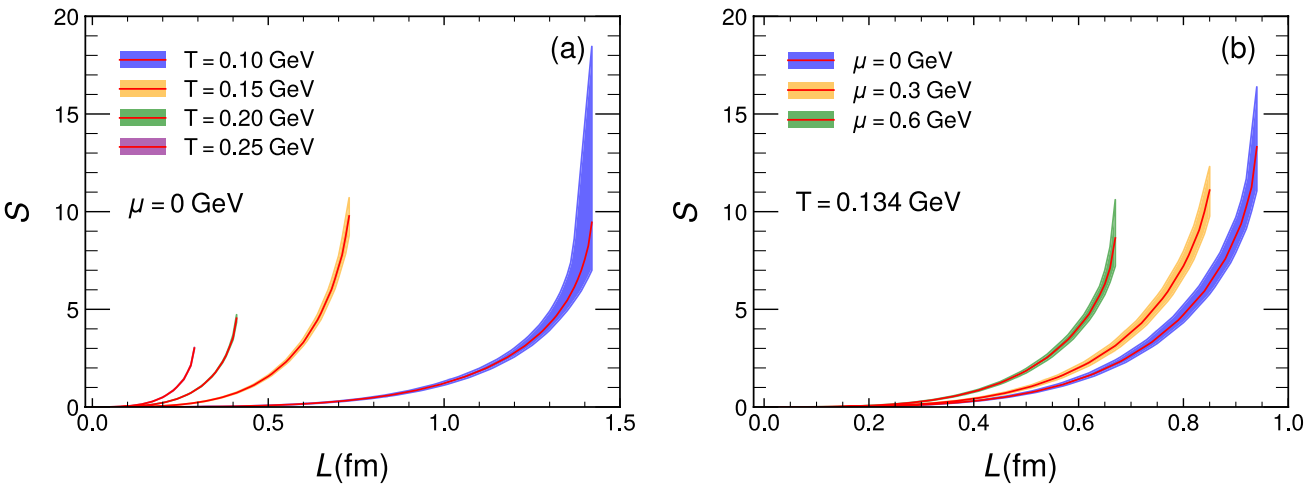

Fig. 4 (Color online) **a** The dependence of the entropy S of quark-antiquark pairs on the interquark distance L at different temperatures when $\mu = 0$. **b** The dependence of the entropy S of quark-antiquark pairs on the interquark distance L at different chemical potential when $T = 0.134$ GeV. The shaded area represents the 95% CL, and the red solid line denotes the result of the MAP calculation

Under specific temperature or chemical potential conditions, an increase in the distance between quarks leads to a significant rise in entropy. This increase in entropy directly results in a larger entropy force, expressed as $F_e = T\frac{\partial S}{\partial L}$ [119]. As shown in Fig. 5, in our calculations, as $L \to L_{max}$, heavy quarkonium approaches dissociation, accompanied by a sharp increase in entropy. According to the definition of entropy, the entropic force corresponds to the derivative of entropy with respect to distance. Consequently, this force tends to infinity under such conditions. In the calculations of Ref. [120], when heavy quarkonium is in the deconfined state, the entropy exhibits a peak, which corresponds to an infinite entropic force. This finding is consistent with our computational results. This phenomenon indicates that the increase in entropy is not merely a thermodynamic characteristic; it is closely related to the dynamic dissociation process of quark-antiquark pairs. As discussed in detail in Ref. [24, 119, 121], the enormous entropy force is considered a key factor driving the dissociation of heavy quark-antiquark pairs, further emphasizing the importance of entropy in the study of quark physics.

3.4 Binding energy

In this section, we use Eq. (32) to calculate the binding energy of heavy quark-antiquark pairs as a function of the distance L between quarks at different temperatures and chemical potentials. As shown in Fig. 6, We calculated the results for the 95% CL (shaded area) and the MAP (red solid line), subfigure (a) displays the calculation results of the effect of different temperatures on the binding energy with the chemical potential fixed at zero, while Subfigure (b) presents the calculation results of the effect of chemical potential on the binding energy with the temperature fixed at $T = 0.134$ GeV. The binding energy increases with rising temperature and chemical potential. When L reaches the critical value L_c (where $L_c \leq L_{max}$), the binding energy becomes zero, indicating that the potential energy of the bound heavy quark-antiquark pair is equal to the free energy of the unbound pair, that is, $E(L_c) = 0$. When L exceeds this critical value L_c, the binding energy becomes positive, indicating that the potential energy of the bound heavy quark-antiquark pair is higher than the free energy of the unbound pair. Notably, a physical distinction exists between the position of zero binding energy L_c and the actual dissociation distance L_{max}. L_c marks a thermodynamic critical point where the free energies of the bound state and the free quark states become equal. However, the heavy quark-antiquark pair does not dissociate at $L > L_c$, but continues to exist as a metastable bound state [18, 39], for further discussion on this issue, see e.g. Ref. [122]. True dissociation occurs at L_{max}, which constitutes a dynamic instability point. When the distance exceeds L_{max}, the string configuration connecting the quark pair becomes dynamically unstable (i.e., 'string snapping'), leading to the dissociation of heavy quarkonium. Consequently, the relationship between these two distances satisfies $L_c < L_{max}$. As shown in Fig. 6, in our calculations the increase in temperature and chemical potential reduces the maximum value of the binding energy. However, we emphasize the effects of temperature and chemical potential on the binding energy at a fixed distance. At a fixed distance, the binding energy increases with rising temperature and chemical potential, while the corresponding absolute value of the binding energy decreases. Simultaneously, the increase in temperature and chemical potential also reduces L_c, indicating that elevated temperature and

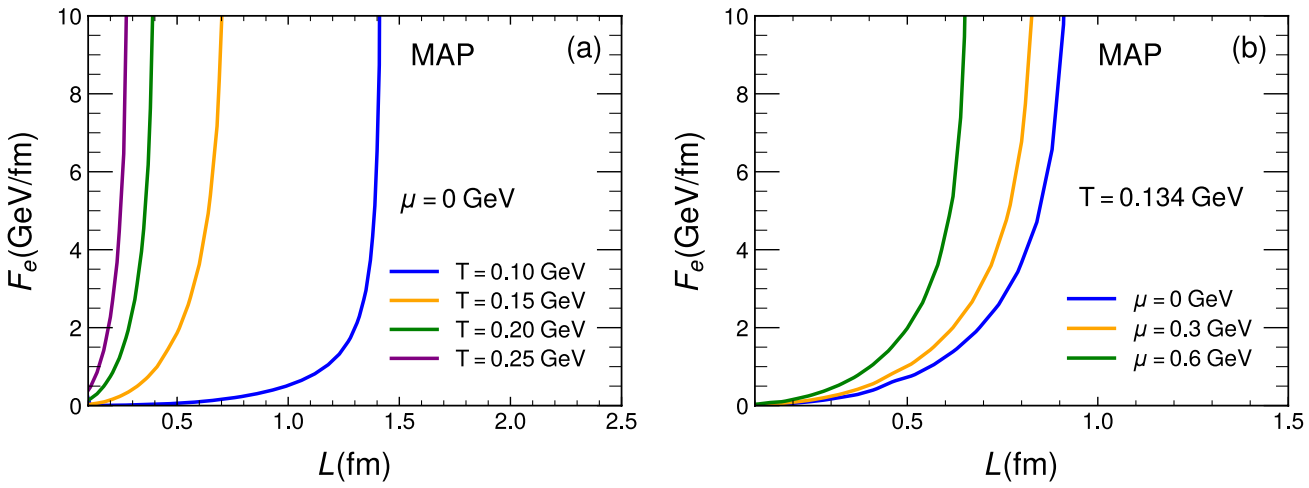

Fig. 5 (Color online) When selecting MAP value, **a** The dependence of the entropy force F_e on interquark distance L for the quark-antiquark pair at different temperatures when $\mu = 0$. **b** The dependence of the entropy force F_e on interquark distance L for the quark-antiquark pair at different chemical potentials when $T = 0.134$ GeV

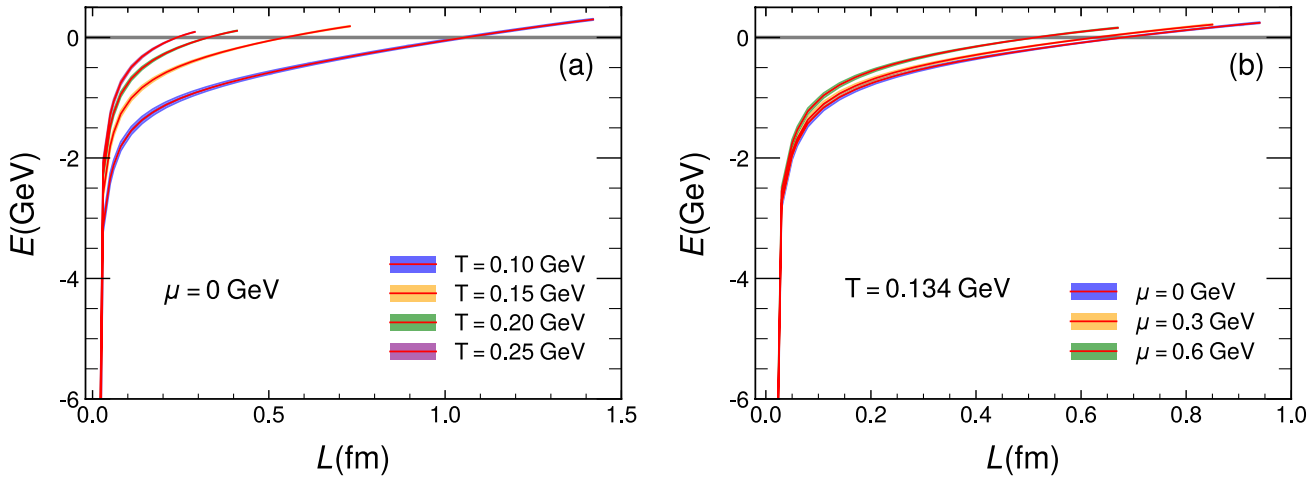

Fig. 6 (Color online) **a** The dependence of the binding energy E of quark-antiquark pairs on the interquark distance L at different temperatures when $\mu = 0$. **b** The dependence of the binding energy E of quark-antiquark pairs on the interquark distance L at different chemical potential when $T = 0.134$ GeV. The shaded area represents the 95% CL, and the red solid line denotes the result of the MAP calculation

chemical potential promote the dissociation of the heavy quarkonium.

3.5 Internal energy

In this section, we employ Eq. (34) to calculate the relationship between the internal energy of heavy quark-antiquark pairs and the interquark distance L under varying temperatures and chemical potentials. As depicted in Fig. 7, We calculated the results for the 95% CL (shaded area) and the MAP (red solid line), subfigure (a) displays the calculation results of the effect of different temperatures on the internal energy with the chemical potential fixed at zero, while subfigure (b) presents the calculation results of the effect of chemical potential on the internal energy with the temperature fixed at $T = 0.134$ GeV. The results indicate that at smaller interquark distances L, the internal energy U is negative and remains relatively unaffected by changes in temperature and chemical potential. However, at larger interquark distances L, the internal energy becomes positive and increases with rising temperature and chemical potential. According to the definition of internal energy, this behavior

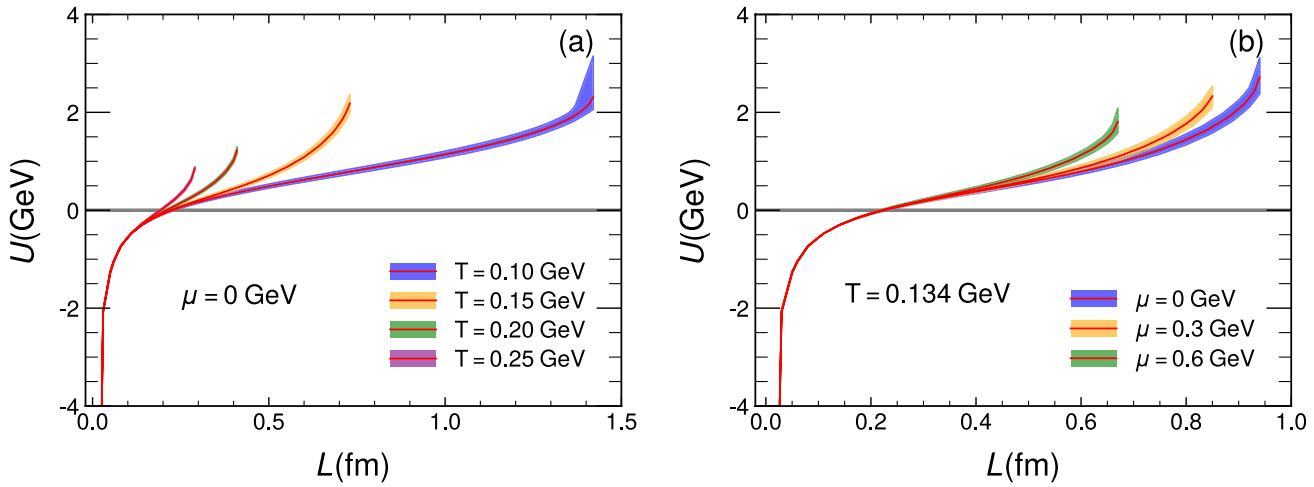

Fig. 7 (Color online) **a** The dependence of the internal energy U of quark-antiquark pairs on the interquark distance L at different temperatures when $\mu = 0$. **b** The dependence of the internal energy U of quark-antiquark pairs on the interquark distance L at different chemical potential when $T = 0.134$ GeV. The shaded area represents the 95% CL, and the red solid line denotes the result of the MAP calculation

suggests that at short interquark distances, the internal energy is predominantly governed by the potential energy, whereas at larger distances, the entropy contributions play a significant role.

4 Thermodynamics of single quark

In this section, we investigate the free energy of a single quark, as shown in Eq. (33), as well as the entropy and internal energy, with the following expressions:

$$S_Q = -\frac{\partial F_Q}{\partial T} = -\frac{\partial F_Q}{\partial z_0}\frac{\partial z_0}{\partial T}, \tag{37}$$

$$U_Q = F_Q + TS_Q. \tag{38}$$

In this section, we investigate the effect of the chemical potential on the thermodynamic quantities of a single quark. We have calculated the results for the 95% CL (shaded area with color) and the maximum a posteriori estimate (red solid line). The free energy of a single quark is shown in Fig. 8, where it can be seen that an increase in chemical potential leads to an increase in free energy, and F_Q/T approaches a conformal situation in the high-temperature limit. The entropy of a single quark is illustrated in Fig. 9, where the results indicate that S_Q also increases with the chemical potential and will tend toward conformal limit in the high-temperature limit. The internal energy of a single quark is shown in Fig. 10, and the results also indicate that the internal energy increases with the chemical potential, with U_Q/T also approaching the conformality limit in the high-temperature limit.

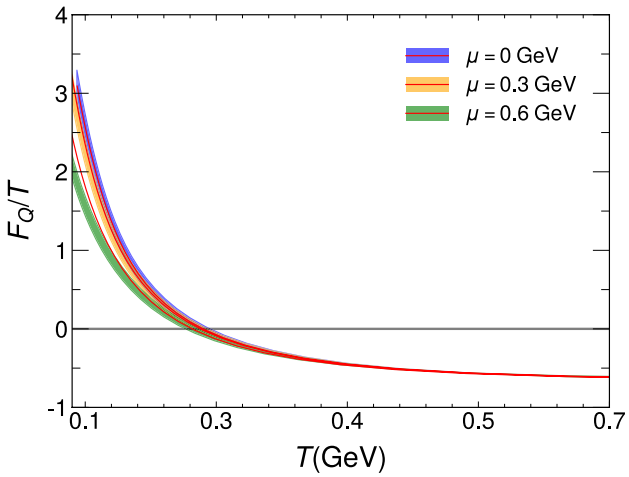

Fig. 8 (Color online) The dependence of the single quark free energy on the temperature for different chemical potentials. The shaded area with color represents the 95% CL, and the red solid line denotes the result of the MAP calculation

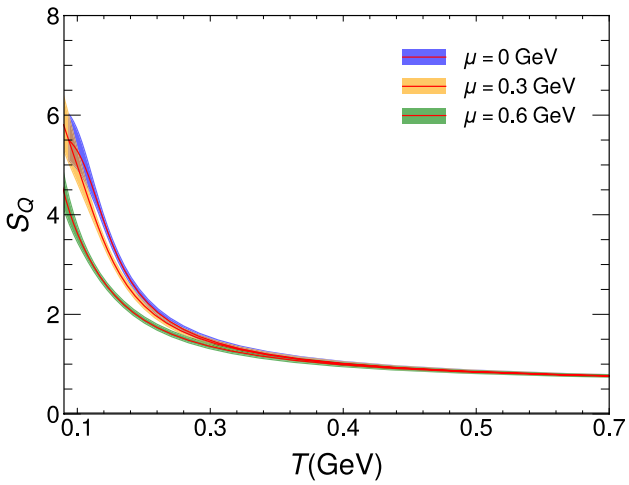

Fig. 9 The dependence of the single quark entropy on the temperature for different chemical potentials. The shaded area with color represents the 95% CL, and the red solid line denotes the result of the MAP calculation

5 Summary

In this study, we investigated the effects of temperature and chemical potential on the dissociation distance, potential energy, entropy, binding energy, and internal energy of heavy quarkonium based on a Bayesian holographic QCD model. Our study finds that an increase in temperature and chemical potential decrease the dissociation distance and suppress the heavy quark potential. When the interquark distance L is small, the effects of temperature and chemical potential on the potential energy are minimal; however, they become more pronounced when the interquark distance L is large. An increase in the temperature and chemical potential results in an increase in the entropy. Within the dissociation distance, the entropy also increases significantly with the interquark distance, leading to a larger entropic force. This larger entropy force facilitates the dissociation of heavy quark-antiquark bound states. Correspondingly, the binding energy reaches zero at smaller interquark distance L as temperature and chemical potential increase, indicating that under high-temperature and high-chemical potential, the binding force of heavy quark-antiquark pairs becomes weaker. The internal energy increases with rising temperature and chemical potential. At smaller interquark distance L, the internal energy is primarily dominated by potential energy, whereas at larger interquark distance L, it is dominated by TS. The effects of temperature and chemical potential on the internal

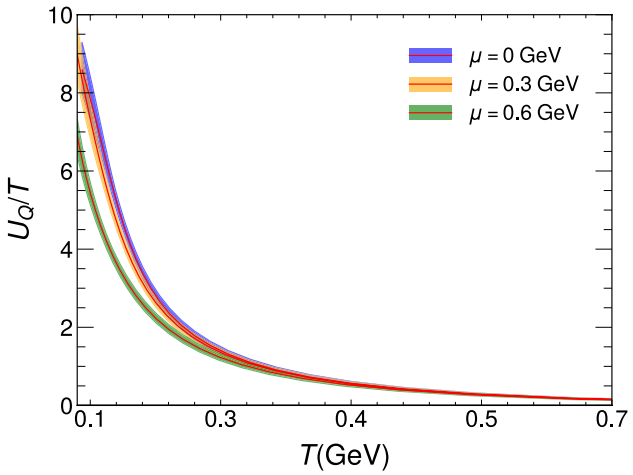

Fig. 10 (Color online) The dependence of the single quark internal energy on the temperature for different chemical potentials. The shaded area with color represents the 95% CL, and the red solid line denotes the result of the MAP calculation

energy are minimal at small quark interquark distance, but become significant at larger interquark distance.

Our results robustly demonstrate that elevated temperature and chemical potential accelerate heavy quarkonium dissociation by enhancing entropic forces and suppressing binding energy. These findings deepen our understanding of quark-gluon plasma (QGP) signatures in heavy-ion collisions and provide a framework for probing QCD matter under extreme conditions. The consistency of the single-quark free energy and entropy trends further supports the generality of our conclusions.

It should be noted that within the holographic model framework, the model parameters obtained from lattice QCD thermodynamic data at zero chemical potential can be utilized to compute the thermodynamic quantities at a finite chemical potential. In Ref. [123], using the holographic model combined with lattice QCD data for the equation of state and second-order baryon number susceptibility at zero chemical potential, the model parameters were derived (Table 1). Calculations based on these derived parameters agree with the lattice QCD data at zero chemical potential (as shown in Fig. 1). Furthermore, thermodynamic quantities calculated at finite chemical potential using these derived parameters also show good agreement with the corresponding lattice QCD data (as demonstrated in Fig. 2). This approach has been widely adopted in holographic model calculations. Our calculations were also based on this methodology.

Although our model captures the essential features of quarkonium dissociation, several limitations warrant discussion. The Bayesian framework relies on specific assumptions about the holographic dual, which may not fully capture the non-perturbative QCD effects; the chemical potential range studied here is applicable to heavy-ion collision scenarios; however, extensions to neutron star matter or other high-density systems require further exploration.

Author contributions All authors jointly participated in the conception and design of the study. Specific contributions are as follows: Xun Chen proposed the core research concept and constructed the computational program framework; Ou-Yang Luo performed critical modifications and optimizations to the program framework; Li-Qiang Zhu was responsible for program debugging, numerical computations, and data analysis of the results; Kai Zhou, Han-Zhong Zhang, and De-Fu Hou jointly carried out the verification and review of the research findings. The first draft of the manuscript was written by Li-Qiang Zhu, and all authors provided important feedback on successive revisions of the paper. All authors have reviewed and approved the final version for submission.

Declarations

Conflict of interest The authors declare that they have no Conflict of interest.

References

1. K. Adcox, S.S. Adler, S. Afanasiev et al., Formation of dense partonic matter in relativistic nucleus-nucleus collisions at RHIC: Experimental evaluation by the PHENIX collaboration. Nucl. Phys. A **757**, 184–283 (2005). https://doi.org/10.1016/j.nuclphysa.2005.03.086
2. M.M. Aggarwal, Z. Ahammed, A.V. Alakhverdyants et al., An experimental exploration of the QCD phase diagram: The search for the critical point and the onset of deconfinement (2010). arXiv:1007.2613
3. J.H. Chen, X. Dong, X.-H. He et al., Properties of the QCD matter: review of selected results from the relativistic heavy ion collider beam energy scan (RHIC BES) program. Nucl. Sci. Tech. **35**, 214 (2024). https://doi.org/10.1007/s41365-024-01591-2
4. H. Wang, J.-H. Chen, Anisotropy flows in Pb–Pb collisions at LHC energies from parton scatterings with heavy quark trigger. Nucl. Sci. Tech. **33**, 15 (2022). https://doi.org/10.1007/s41365-022-00999-y
5. H. Wang, J.-H. Chen, Study on open charm hadron production and angular correlation in high-energy nuclear collisions. Nucl. Sci. Tech. **32**, 2 (2021). https://doi.org/10.1007/s41365-020-00839-x
6. H. Wang, J.-H. Chen, Y.-G. Ma et al., Charm hadron azimuthal angular correlations in Au + Au collisions at $\sqrt{s_{\rm NN}}$ = 200 GeV from parton scatterings. Nucl. Sci. Tech. **30**, 185 (2019). https://doi.org/10.1007/s41365-019-0706-z
7. Z.-W. Xu, S. Zhang, Y.-G. Ma et al., Influence of α -clustering nuclear structure on the rotating collision system. Nucl. Sci. Tech. **29**, 186 (2018). https://doi.org/10.1007/s41365-018-0523-9
8. X.-H. Jin, J.-H. Chen, Y.-G. Ma et al., Ω and ϕ production in Au + Au collisions at $\sqrt{s_{\rm NN}}$ = 11.5 and 7.7 GeV in a dynamical quark coalescence model. Nucl. Sci. Tech. **29**, 54 (2018). https://doi.org/10.1007/s41365-018-0393-1
9. P. Liu, J.-H. Chen, Y.-G. Ma et al., Production of light nuclei and hypernuclei at High Intensity Accelerator Facility energy region. Nucl. Sci. Tech. **28**, 55 (2017). https://doi.org/10.1007/s41365-017-0207-x. [Erratum: Nucl.Sci.Tech. 28, 89 (2017)]

10. L. Zhu, Z. Gao, W. Ke et al., Bayesian inference of the magnetic field and chemical potential on holographic jet quenching in heavy-ion collisions (2025). arXiv:2506.00340
11. M. Xie, Q.-F. Han, E.-K. Wang et al., The medium-temperature dependence of jet transport coefficient in high-energy nucleus-nucleus collisions. Nucl. Sci. Tech. **35**, 125 (2024). https://doi.org/10.1007/s41365-024-01492-4
12. W.-B. He, Y.-G. Ma, L.-G. Pang et al., High-energy nuclear physics meets machine learning. Nucl. Sci. Tech. **34**, 88 (2023). https://doi.org/10.1007/s41365-023-01233-z
13. Y.-F. Xu, Y.-J. Ye, J.-H. Chen et al., Low-mass vector meson production at forward rapidity in p+p and d+Au collisions at $\sqrt{s_{\rm NN}} = 200$ GeV from a multiphase transport model. Nucl. Sci. Tech. **27**, 87 (2016). https://doi.org/10.1007/s41365-016-0093-7
14. Y.-G. Ma, L.-G. Pang, R. Wang et al., Phase transition study meets machine learning. Chin. Phys. Lett. **40**, 122101 (2023). https://doi.org/10.1088/0256-307X/40/12/122101
15. J. Bulava, B. Hörz, F. Knechtli et al., String breaking by light and strange quarks in QCD. Phys. Lett. B **793**, 493–498 (2019). https://doi.org/10.1016/j.physletb.2019.05.018
16. Y. Li, C.W. von Keyserlingk, G. Zhu et al., Phase diagram of the three-dimensional subsystem toric code. Phys. Rev. Res. **6**, 043007 (2024). https://doi.org/10.1103/PhysRevResearch.6.043007
17. Y. Yang, P.-H. Yuan, Confinement-deconfinement phase transition for heavy quarks in a soft wall holographic QCD model. J. High Energ. Phys. **2015**, 161 (2015). https://doi.org/10.1007/JHEP12(2015)161
18. J. Zhou, X. Chen, Y.-Q. Zhao et al., Thermodynamics of heavy quarkonium in a magnetic field background. Phys. Rev. D **102**, 086020 (2020). https://doi.org/10.1103/PhysRevD.102.086020
19. S. Shi, K. Zhou, J. Zhao et al., Heavy quark potential in the quark-gluon plasma: Deep neural network meets lattice quantum chromodynamics. Phys. Rev. D **105**, 014017 (2022). https://doi.org/10.1103/PhysRevD.105.014017
20. K. Zhou, N. Xu, P. Zhuang, Υ production in heavy ion collisions at LHC. Nucl. Phys. A **931**, 654–658 (2014). https://doi.org/10.1016/j.nuclphysa.2014.08.104
21. K. Zhou, N. Xu, Z. Xu et al., Medium effects on charmonium production at ultrarelativistic energies available at the CERN Large Hadron Collider. Phys. Rev. C **89**, 054911 (2014). https://doi.org/10.1103/PhysRevC.89.054911
22. T. Matsui, H. Satz, J/ψ Suppression by Quark-Gluon Plasma formation. Phys. Lett. B **178**, 416–422 (1986). https://doi.org/10.1016/0370-2693(86)91404-8
23. J.M. Maldacena, Wilson loops in large N field theories. Phys. Rev. Lett. **80**, 4859–4862 (1998). https://doi.org/10.1103/PhysRevLett.80.4859
24. Z.-R. Zhu, S. Wang, X. Chen et al., Thermodynamics of heavy quarkonium in the spinning black hole background. Phys. Rev. D **110**, 126008 (2024). https://doi.org/10.1103/PhysRevD.110.126008. arXiv:2407.03633
25. Z.-R. Zhu, M. Sun, R. Zhou et al., Heavy quarkonium spectral function in the spinning black hole background. Eur. Phys. J. C **84**, 1252 (2024). https://doi.org/10.1140/epjc/s10052-024-13628-2
26. O. Andreev, V.I. Zakharov, Heavy-quark potentials and AdS/QCD. Phys. Rev. D **74**, 025023 (2006). https://doi.org/10.1103/PhysRevD.74.025023
27. O. Andreev, V.I. Zakharov, The spatial string tension, thermal phase transition, and AdS/QCD. Phys. Lett. B **645**, 437–441 (2007). https://doi.org/10.1016/j.physletb.2007.01.002
28. O. Andreev, V.I. Zakharov, On heavy-quark free energies, entropies, polyakov loop, and AdS/QCD. J. High Energ. Phys. **2007**, 100 (2007). https://doi.org/10.1088/1126-6708/2007/04/100
29. S. He, M. Huang, Q.-S. Yan, Heavy quark potential and QCD beta function from a deformed AdS_5 model. Prog. Theor. Phys. Suppl. **186**, 504–509 (2010). https://doi.org/10.1143/PTPS.186.504
30. P. Colangelo, F. Giannuzzi, S. Nicotri, Holography, heavy-quark free energy, and the QCD phase diagram. Phys. Rev. D **83**, 035015 (2011). https://doi.org/10.1103/PhysRevD.83.035015
31. O. DeWolfe, S.S. Gubser, C. Rosen, A holographic critical point. Phys. Rev. D **83**, 086005 (2011). https://doi.org/10.1103/PhysRevD.83.086005
32. D. Li, S. He, M. Huang et al., Thermodynamics of deformed AdS_5 model with a positive/negative quadratic correction in graviton-dilaton system. J. High Energ. Phys. **2011**, 041 (2011). https://doi.org/10.1007/JHEP09(2011)041
33. K.B. Fadafan, Heavy quarks in the presence of higher derivative corrections from AdS/CFT. Eur. Phys. J. C **71**, 1799 (2011). https://doi.org/10.1140/epjc/s10052-011-1799-7
34. K.B. Fadafan, E. Azimfard, On meson melting in the quark medium. Nucl. Phys. B **863**, 347–360 (2012). https://doi.org/10.1016/j.nuclphysb.2012.05.022
35. R.-G. Cai, S. He, D. Li, A hQCD model and its phase diagram in Einstein-Maxwell-Dilaton system. J. High Energ. Phys. **2012**, 033 (2012). https://doi.org/10.1007/JHEP03(2012)033
36. D. Li, M. Huang, Q.-S. Yan, A dynamical soft-wall holographic QCD model for chiral symmetry breaking and linear confinement. Eur. Phys. J. C **73**, 2615 (2013). https://doi.org/10.1140/epjc/s10052-013-2615-3
37. Z. Fang, S. He, D. Li, Chiral and Deconfining Phase Transitions from Holographic QCD Study. Nucl. Phys. B **907**, 187–207 (2016). https://doi.org/10.1016/j.nuclphysb.2016.04.003
38. Z.-Q. Zhang, D.-F. Hou, G. Chen, Heavy quark potential from deformed AdS_5 models. Nucl. Phys. A **960**, 1–10 (2017). https://doi.org/10.1016/j.nuclphysa.2017.01.007
39. C. Ewerz, O. Kaczmarek, A. Samberg, Free energy of a heavy quark-antiquark pair in a thermal medium from AdS/CFT. J. High Energ. Phys. **2018**, 088 (2018). https://doi.org/10.1007/JHEP03(2018)088
40. X. Chen, S.-Q. Feng, Y.-F. Shi et al., Moving heavy quarkonium entropy, effective string tension, and the QCD phase diagram. Phys. Rev. D **97**, 066015 (2018). https://doi.org/10.1103/PhysRevD.97.066015
41. I. Aref'eva, K. Rannu, Holographic anisotropic background with confinement-deconfinement phase transition. J. High Energ. Phys. **2018**, 206 (2018). https://doi.org/10.1007/JHEP05(2018)206
42. X. Chen, D. Li, M. Huang, Criticality of QCD in a holographic QCD model with critical end point. Chin. Phys. C **43**, 023105 (2019). https://doi.org/10.1088/1674-1137/43/2/023105
43. H. Bohra, D. Dudal, A. Hajilou et al., Anisotropic string tensions and inversely magnetic catalyzed deconfinement from a dynamical AdS/QCD model. Phys. Lett. B **801**, 135184 (2020). https://doi.org/10.1016/j.physletb.2019.135184
44. X. Chen, D. Li, D. Hou et al., Quarkyonic phase from quenched dynamical holographic QCD model. J. High Energ. Phys. **2020**, 073 (2020). https://doi.org/10.1007/JHEP03(2020)073
45. J. Zhou, X. Chen, Y.-Q. Zhao et al , Thermodynamics of heavy quarkonium in rotating matter from holography. Phys. Rev. D **102**, 126029 (2021). https://doi.org/10.1103/PhysRevD.102.126029
46. X. Chen, L. Zhang, D. Li et al., Gluodynamics and deconfinement phase transition under rotation from holography. J. High Energ. Phys. **2021**, 132 (2021). https://doi.org/10.1007/JHEP07(2021)132
47. X. Chen, L. Zhang, D. Hou, Running coupling constant at finite chemical potential and magnetic field from holography *. Chin.

Phys. C **46**, 073101 (2022). https://doi.org/10.1088/1674-1137/ac5c2d
48. Z. Fodor, S.D. Katz, A New method to study lattice QCD at finite temperature and chemical potential. Phys. Lett. B **534**, 87–92 (2002). https://doi.org/10.1016/S0370-2693(02)01583-6
49. An Introductory review, S. Muroya, A. Nakamura, C. Nonaka T. Takaishi, Lattice QCD at finite density. Prog. Theor. Phys. **110**, 615–668 (2003). https://doi.org/10.1143/PTP.110.615
50. C.B. Lang, C. Rebbi, Potential and Restoration of Rotational Symmetry in SU(2) Lattice Gauge Theory. Phys. Lett. B **115**, 137 (1982). https://doi.org/10.1016/0370-2693(82)90813-9
51. J. Hoek, Wilson Loops on 32**4 Lattices and the SU(3) Potential. Z. Phys. C **35**, 369–377 (1987). https://doi.org/10.1007/BF01570774
52. C. Michael, S.J. Perantonis, Potentials and glueballs at large beta in SU(2) pure gauge theory. J. Phys. G **18**, 1725–1736 (1992). https://doi.org/10.1088/0954-3899/18/11/005
53. T.T. Takahashi, H. Suganuma, Y. Nemoto et al., Detailed analysis of the three quark potential in SU(3) lattice QCD. Phys. Rev. D **65**, 114509 (2002). https://doi.org/10.1103/PhysRevD.65.114509
54. Y. Aoki, Z. Fodor, S.D. Katz et al., The Equation of state in lattice QCD: With physical quark masses towards the continuum limit. J. High Energ. Phys. **2006**, 089 (2006). https://doi.org/10.1088/1126-6708/2006/01/089
55. C. Ratti, M.A. Thaler, W. Weise, Phases of QCD: Lattice thermodynamics and a field theoretical model. Phys. Rev. D **73**, 014019 (2006). https://doi.org/10.1103/PhysRevD.73.014019
56. P. Bicudo, M. Cardoso, O. Oliveira, Study of the gluon-quark-antiquark static potential in SU(3) lattice QCD. Phys. Rev. D **77**, 091504 (2008). https://doi.org/10.1103/PhysRevD.77.091504
57. M. Lüscher, Properties and uses of the Wilson flow in lattice QCD. J. High Energ. Phys. **2010**, 071 (2010). https://doi.org/10.1007/JHEP08(2010)071. (**[Erratum: J. High Energ. Phys. 2014, 092 (2014)]**)
58. P. Hasenfratz, F. Karsch, Chemical Potential on the Lattice. Phys. Lett. B **125**, 308–310 (1983). https://doi.org/10.1016/0370-2693(83)91290-X
59. J.-J. Jiang, Y.-Z. Xiao, J. Qin et al., Three-quark potential at finite temperature and chemical potential*. Chin. Phys. C **47**, 013106 (2023). https://doi.org/10.1088/1674-1137/ac9894
60. B. Yu, X. Guo, X. Chen et al., Potential and string breaking of doubly heavy baryon at finite temperature and chemical potential. Phys. Rev. D **108**, 066007 (2023). https://doi.org/10.1103/PhysRevD.108.066007
61. K. Zhou, L. Wang, L.-G. Pang et al., Exploring QCD matter in extreme conditions with machine learning. Prog. Part. Nucl. Phys. **135**, 104084 (2024). https://doi.org/10.1016/j.ppnp.2023.104084
62. S. He, M. Huang, Q.-S. Yan et al., Confront holographic QCD with regge trajectories. Eur. Phys. J. C **66**, 187–196 (2010). https://doi.org/10.1140/epjc/s10052-010-1239-0
63. B.A. Burrington, J.T. Liu, L.A. Pando Zayas et al., Holographic duals of flavored N=1 super Yang-mills: Beyond the probe approximation. J. High Energ. Phys. **2005**, 022 (2005). https://doi.org/10.1088/1126-6708/2005/02/022
64. T. Sakai, S. Sugimoto, More on a holographic dual of QCD. Prog. Theor. Phys. **114**, 1083–1118 (2005). https://doi.org/10.1143/PTP.114.1083
65. T. Sakai, S. Sugimoto, Low energy hadron physics in holographic QCD. Prog. Theor. Phys. **113**, 843–882 (2005). https://doi.org/10.1143/PTP.113.843
66. J. Erdmenger, N. Evans, W. Porod et al., Gauge/gravity dynamics for composite Higgs models and the top mass. Phys. Rev. Lett. **126**, 071602 (2021). https://doi.org/10.1103/PhysRevLett.126.071602
67. N.R.F. Braga, Ra. da Rocha, AdS/QCD duality and the quarkonia holographic information entropy. Phys. Lett. B **776**, 78–83 (2018). https://doi.org/10.1016/j.physletb.2017.11.034
68. N.R.F. Braga, L.F. Ferreira, Ra. Da Rocha, Thermal dissociation of heavy mesons and configurational entropy. Phys. Lett. B **787**, 16–22 (2018). https://doi.org/10.1016/j.physletb.2018.10.036
69. L.F. Ferreira, R. da Rocha, Tensor mesons, AdS/QCD and information. Eur. Phys. J. C **80**, 375 (2020). https://doi.org/10.1140/epjc/s10052-020-7978-7
70. S. He, M. Huang, Q.-S. Yan, Logarithmic correction in the deformed AdS_5 model to produce the heavy quark potential and QCD beta function. Phys. Rev. D **83**, 045034 (2011). https://doi.org/10.1103/PhysRevD.83.045034
71. N. Jokela, M. Järvinen, A. Piispa, Refining holographic models of the quark-gluon plasma. Phys. Rev. D **110**, 126013 (2024). https://doi.org/10.1103/PhysRevD.110.126013
72. HIC in Holographic Approach, I. Y. Aref'eva, HQCD. Phys. Part. Nucl. **54**, 924–930 (2023). https://doi.org/10.1134/S1063779623050039
73. R. Rougemont, J. Grefa, M. Hippert et al., Hot QCD phase diagram from holographic Einstein-Maxwell-Dilaton models. Prog. Part. Nucl. Phys. **135**, 104093 (2024). https://doi.org/10.1016/j.ppnp.2023.104093
74. S.-J. Rey, S. Theisen, J.-T. Yee, Wilson-Polyakov loop at finite temperature in large N gauge theory and anti-de Sitter supergravity. Nucl. Phys. B **527**, 171–186 (1998). https://doi.org/10.1016/S0550-3213(98)00471-4
75. A. Brandhuber, N. Itzhaki, J. Sonnenschein et al., Wilson loops in the large N limit at finite temperature. Phys. Lett. B **434**, 36–40 (1998). https://doi.org/10.1016/S0370-2693(98)00730-8
76. J. Noronha, The heavy quark free energy in QCD and in Gauge theories with gravity duals. Phys. Rev. D **82**, 065016 (2010). https://doi.org/10.1103/PhysRevD.82.065016
77. Z.-Q. Zhang, C. Ma, D.-F. Hou et al., Heavy quark potential with hyperscaling violation. Adv. High Energy Phys. **2017**, 8276534 (2017). https://doi.org/10.1155/2017/8276534
78. X. Chen, B. Yu, P.-C. Chu et al., Studying the potential of QQq at finite temperature in a holographic model *. Chin. Phys. C **46**, 073102 (2022). https://doi.org/10.1088/1674-1137/ac5db9
79. X. Guo, J.-J. Jiang, X. Liu et al., Doubly-heavy tetraquark at finite temperature in a holographic model. Eur. Phys. J. C **84**, 101 (2024). https://doi.org/10.1140/epjc/s10052-024-12453-x
80. I. Iatrakis, D.E. Kharzeev, Holographic entropy and real-time dynamics of quarkonium dissociation in non-Abelian plasma. Phys. Rev. D **93**, 086009 (2016). https://doi.org/10.1103/PhysRevD.93.086009
81. S.S. Jena, B. Shukla, D. Dudal et al.,, Entropic force and real-time dynamics of holographic quarkonium in a magnetic field. Phys. Rev. D **105**, 086011 (2022). https://doi.org/10.1103/PhysRevD.105.086011
82. T. Song, Y. Park, S.H. Lee et al., The Thermal width of heavy quarkonia moving in quark gluon plasma. Phys. Lett. B **659**, 621–627 (2008). https://doi.org/10.1016/j.physletb.2007.11.084
83. M.A. Escobedo, F. Giannuzzi, M. Mannarelli et al., Heavy Quarkonium moving in a Quark-Gluon Plasma. Phys. Rev. D **87**, 114005 (2013). https://doi.org/10.1103/PhysRevD.87.114005
84. X. Chen, M. Huang, Machine learning holographic black hole from lattice QCD equation of state. Phys. Rev. D **109**, L051902 (2024). https://doi.org/10.1103/PhysRevD.109.L051902
85. X. Chen, M. Huang, Flavor dependent critical endpoint from holographic QCD through machine learning (2024). arXiv:2405.06179
86. L. Zhu, X. Chen, K. Zhou et al., Bayesian inference of the critical end point in a (2+1)-flavor system from holographic QCD. Phys. Rev. D **112**, 026019 (2025). https://doi.org/10.1103/wpts-lbtr

87. S. He, S.-Y. Wu, Y. Yang et al., Phase structure in a dynamical soft-wall holographic QCD model. J. High Energ. Phys. **2013**, 093 (2013). https://doi.org/10.1007/JHEP04(2013)093
88. Y. Yang, P.-H. Yuan, A refined holographic QCD model and QCD phase structure. J. High Energ. Phys. **2014**, 149 (2014). https://doi.org/10.1007/JHEP11(2014)149
89. D. Dudal, S. Mahapatra, Thermal entropy of a quark-antiquark pair above and below deconfinement from a dynamical holographic QCD model. Phys. Rev. D **96**, 126010 (2017). https://doi.org/10.1103/PhysRevD.96.126010
90. D. Dudal, S. Mahapatra, Interplay between the holographic QCD phase diagram and entanglement entropy. J. High Energ. Phys. **2018**, 120 (2018). https://doi.org/10.1007/JHEP07(2018)120
91. R. Critelli, J. Noronha, J. Noronha-Hostler et al., Critical point in the phase diagram of primordial quark-gluon matter from black hole physics. Phys. Rev. D **96**, 096026 (2017). https://doi.org/10.1103/PhysRevD.96.096026
92. L. Zhang, M. Huang, Holographic cold dense matter constrained by neutron stars. Phys. Rev. D **106**, 096028 (2022). https://doi.org/10.1103/PhysRevD.106.096028
93. S.W. Hawking, D.N. Page, Thermodynamics of black holes in anti-de sitter space. Commun. Math. Phys. **87**, 577 (1983). https://doi.org/10.1007/BF01208266
94. M. Natsuume, AdS/CFT duality user guide. Springer Tokyo, (2015). https://doi.org/10.1007/978-4-431-55441-7
95. E. Witten, Anti-de sitter space, thermal phase transition, and confinement in gauge theories. Adv. Theor. Math. Phys. **2**, 505–532 (1998). https://doi.org/10.4310/ATMP.1998.v2.n3.a3
96. A. Brandhuber, N. Itzhaki, J. Sonnenschein et al., Wilson loops, confinement, and phase transitions in large N gauge theories from supergravity. J. High Energ. Phys. **1998**, 001 (1998). https://doi.org/10.1088/1126-6708/1998/06/001
97. D.J. Gross, H. Ooguri, Aspects of large N gauge theory dynamics as seen by string theory. Phys. Rev. D **58**, 106002 (1998). https://doi.org/10.1103/PhysRevD.58.106002
98. D. Giataganas, N. Irges, Flavor corrections in the static potential in holographic QCD. Phys. Rev. D **85**, 046001 (2012). https://doi.org/10.1103/PhysRevD.85.046001
99. S.-J. Rey, J.-T. Yee, Macroscopic strings as heavy quarks in large N gauge theory and anti-de Sitter supergravity. Eur. Phys. J. C **22**, 379–394 (2001). https://doi.org/10.1007/s100520100799
100. A. Mocsy, P. Petreczky, Can quarkonia survive deconfinement? Phys. Rev. D **77**, 014501 (2008). https://doi.org/10.1103/PhysRevD.77.014501. arXiv:0705.2559
101. H. Satz, Quarkonium binding and entropic force. Eur. Phys. J. C **75**, 193 (2015). https://doi.org/10.1140/epjc/s10052-015-3424-7
102. G.S. Bali, F. Bruckmann, G. Endrodi et al., The QCD phase diagram for external magnetic fields. J. High Energ. Phys. **2012**, 044 (2012). https://doi.org/10.1007/JHEP02(2012)044
103. A. Bazavov, T. Bhattacharya, C. DeTar et al., Equation of state in (2+1)-flavor QCD. Phys. Rev. D **90**, 094503 (2014). https://doi.org/10.1103/PhysRevD.90.094503
104. A. Bazavov, H.-T. Ding, P. Hegde et al., The QCD Equation of State to $O(\mu_B^6)$ from Lattice QCD. Phys. Rev. D **95**, 054504 (2017). https://doi.org/10.1103/PhysRevD.95.054504
105. B. Tang, Orthogonal array-based latin hypercubes. J. Am. Stat. Assoc. **88**, 1392–1397 (1993)
106. M.D. Morris, T.J. Mitchell, Exploratory designs for computational experiments. J. Statist. Plan. Inf. **43**, 381–402 (1995). https://doi.org/10.1016/0378-3758(94)00035-T
107. M. E. Tipping, C. M. Bishop, Mixtures of probabilistic principal component analyzers. Neural Computation 11, 443–482 (1999). https://doi.org/10.1162/089976699300016728
108. C.K. Williams, C.E. Rasmussen, *Gaussian processes for machine learning 2* (MIT press Cambridge, MA, 2006)
109. D. Foreman-Mackey, D.W. Hogg, D. Lang et al., Emcee: the MCMC hammer. Public. Astro. Soc. Pacific **125**(925), 306 (2013). https://doi.org/10.1086/670067
110. J. Goodman, J. Weare, Ensemble samplers with affine invariance. Commun. Appl. Math. Comput. Sc. **5**, 65–80 (2010). https://doi.org/10.2140/camcos.2010.5.65
111. N. Brambilla, J. Ghiglieri, A. Vairo et al., Static quark-antiquark pairs at finite temperature. Phys. Rev. D **78**, 014017 (2008). https://doi.org/10.1103/PhysRevD.78.014017
112. M. Laine, O. Philipsen, P. Romatschke et al., Real-time static potential in hot QCD. JHEP **03**, 054 (2007). https://doi.org/10.1088/1126-6708/2007/03/054
113. S.I. Finazzo, J. Noronha, Thermal suppression of moving heavy quark pairs in a strongly coupled plasma. J. High Energ. Phys. **2015**, 051 (2015). https://doi.org/10.1007/JHEP01(2015)051. arXiv:1406.2683
114. R.N. Larsen, G. Parkar, A. Rothkopf et al., In-medium static inter-quark potential on high resolution quenched lattices. Phys. Rev. D **110**, 114501 (2024). https://doi.org/10.1103/PhysRevD.110.114501. arXiv:2402.10819
115. D.J. Gross, F. Wilczek, Ultraviolet behavior of nonabelian Gauge theories. Phys. Rev. Lett. **30**, 1343–1346 (1973). https://doi.org/10.1103/PhysRevLett.30.1343
116. H.D. Politzer, Reliable perturbative results for strong interactions? Phys. Rev. Lett. **30**, 1346–1349 (1973). https://doi.org/10.1103/PhysRevLett.30.1346
117. G.T. Hooft, The birth of asymptotic freedom. Nucl. Phys. B **254**, 11–18 (1985). https://doi.org/10.1016/0550-3213(85)90206-8
118. A. Bazavov, D. Hoying, R.N. Larsen et al., Unscreened forces in the quark-gluon plasma? Phys. Rev. D **109**, 074504 (2024). https://doi.org/10.1103/PhysRevD.109.074504
119. D.E. Kharzeev, Deconfinement as an entropic self-destruction: a solution for the quarkonium suppression puzzle? Phys. Rev. D **90**, 074007 (2014). https://doi.org/10.1103/PhysRevD.90.074007
120. K. Hashimoto, D.E. Kharzeev, Entropic destruction of heavy quarkonium in non-Abelian plasma from holography. Phys. Rev. D **90**, 125012 (2014). https://doi.org/10.1103/PhysRevD.90.125012. arXiv:1411.0618
121. P.-P. Wu, Z.-Q. Zhang, X. Zhu, Entropic destruction of heavy quarkonium in a rotating hot and dense medium from holography*. Chin. Phys. C **46**, 113103 (2022). https://doi.org/10.1088/1674-1137/ac814e
122. J.J. Friess, S.S. Gubser, G. Michalogiorgakis et al., Stability of strings binding heavy-quark mesons. J. High Energ. Phys. **2007**, 079 (2007). https://doi.org/10.1088/1126-6708/2007/04/079
123. Z. Li, F. Wang, Phase transition of hot dense QCD Matter from a refined holographic EMD model (2025). arXiv:2507.09113

Authors and Affiliations

Li-Qiang Zhu[1] · Ou-Yang Luo[2] · Xun Chen[1,2,3,4] · Kai Zhou[5,6] · Han-Zhong Zhang[1] · De-Fu Hou[1]

✉ Li-Qiang Zhu
zhuliqiang@mails.ccnu.edu.cn

✉ Ou-Yang Luo
luoouyangedu@qq.com

✉ Xun Chen
chenxun@usc.edu.cn

✉ Kai Zhou
zhoukai@cuhk.edu.cn

✉ Han-Zhong Zhang
zhanghz@mail.ccnu.edu.cn

✉ De-Fu Hou
houdf@mail.ccnu.edu.cn

[1] Key Laboratory of Quark and Lepton Physics (MOE) and Institute of Particle Physics, Central China Normal University, Wuhan 430079, China

[2] School of Nuclear Science and Technology, University of South China, Hengyang 421001, China

[3] Key Laboratory of Advanced Nuclear Energy Design and Safety, Ministry of Education, Hengyang 421001, China

[4] INFN - Istituto Nazionale di Fisica Nucleare - Sezione di Bari, Via Orabona 4, 70125 Bari, Italy

[5] School of Science and Engineering, The Chinese University of Hong Kong (CUHK-Shenzhen), Shenzhen 518172, China

[6] School of Artificial Intelligence, The Chinese University of Hong Kong (CUHK-Shenzhen), Shenzhen 518172, China